DETERMINATION OF THE DONOR PAIR EXCHANGE ENERGY IN PHOSPHORUS-DOPED SILICON

by

PIETER RUTTER CULLIS

A THESIS SUBMITTED IN PARTIAL FULFILMENT OF
THE REQUIREMENTS FOR THE DEGREE OF
MASTER OF SCIENCE

in the Department
of
Physics

We accept this thesis as conforming to the
required standard

THE UNIVERSITY OF BRITISH COLUMBIA
April, 1970

In presenting this thesis in partial fulfilment of the requirements for an advanced degree at the University of British Columbia, I agree that the Library shall make it freely available for reference and study. I further agree tha permission for extensive copying of this thesis for scholarly purposes may be granted by the Head of my Department or by his representatives. It is understood that copying or publication of this thesis for financial gain shall not be allowed without my written permission.

Department of Physics

The University of British Columbia
Vancouver 8, Canada

Date April 17, 1970

ABSTRACT

The e.p.r. spectrum for relatively dilute samples of phosphorus-doped silicon ($<5 \times 10^{16}$ donors/cm^3) has been calculated in detail for an assumed random distribution of impurities. The system of donor electron spins is treated as a collection of nearest neighbor donor pairs. An expression is derived for the donor pair exchange energy using Kohn-Luttinger wavefunctions and a general exchange energy expression. The resultant relationship contains an adjustable parameter a^*, the "effective Bohr radius", which is determined from a comparison of the calculated spectrum and the experimental results obtained for the ratio, C, of the "central pair" and "hyperfine" line intensities. The resulting expression $J(\underline{R})$, where J represents the exchange energy and $\underline{R}$ the separation vector connecting the two pair donors, exhibits an oscillatory spatial dependence due to interference from portions of the wavefunction arising from different conduction band valleys.

TABLE OF CONTENTS

LIST OF FIGURES

LIST OF TABLES

ACKNOWLEDGEMENTS

I would like to thank Dr. John R. Marko for his suggestion of the thesis topic and subsequent encouragement through all phases of the problem.

Thanks also go to Dr. R. Barrie, who was a critical sounding-board for many aspects of this thesis.

I would like to express gratitude to the National Research Council for their award of a Post Graduate Studentship for the duration of this work.

The research for this thesis was supported by the National Research Council, Grant Number 67-4624.

CHAPTER I

INTRODUCTION

The electron spin resonance (E.S.R.) spectrum of phosphorus doped silicon (P-Si) in the concentration range $10^{15} < N < 10^{18}$ impurities /cm^3 demonstrates a "weak centre peak" that lies midway between the hyperfine lines of the isolated donors. Slichter[1] attributed this peak to coupled pairs of neighbouring impurities that act as a unit with a total spin of 1. In samples with $N_d < 5 \times 10^{16}$/cm^3 ancillary lines adjacent to the centre peak have similarly been explained in terms of clusters of three or more donor atoms.

The degree to which two interacting spins may be considered to act as a pair is given by the exchange energy "J" between them. Slichter's calculation included only those pairs for which $J \sim A$, where A is the hyperfine interaction. It is the purpose of this work to determine the functional dependence of J on "r", the interdonor separation, for all values of r. This functional dependence is constructed so as to contain a single adjustable parameter a^*, the "effective Bohr radius" of the impurity electron, which is subsequently fitted to experimental results.

Motivation for the determination of J arises partly from the "spin diffusion" mechanism that can transport energy from one part of a spectral line to another[2], presumably via a flip-flop of neighbouring spins. It has been proposed that the bulk of electronic spins relax through such a diffusion of spin and energy to other spin centres with very short spin lattice relaxation times, "T_1". One of these fast relaxing centres is suspected to be[3] the previously mentioned highly coupled pair, with $T_1 \propto J^{-2}$. A functional knowledge of J is therefore essential before detailed studies of the spin diffusion relaxation mechanism can be initiated.

Attention has also been given to a broad background line that

has been observed beneath the isolated donor spectrum of P-Si and which extends well outside this spectrum. This line is thought to arise from exchange coupled pairs for which $J \sim A$. It is shown that at least part of this line is due to such pairs.

CHAPTER II

THEORY

A. Electron Spin Resonance

The basic energy levels of the unpaired electrons of a paramagnetic sample in a magnetic field $\underline{H}=H_0\hat{k}$ are given in Figure 1.

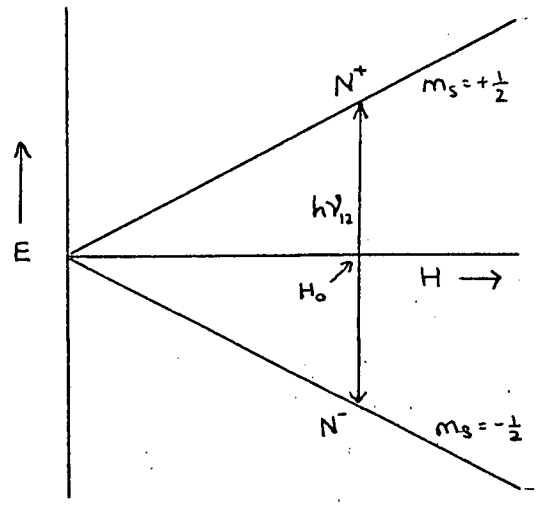

m_s=the electronic spin quantum number
$h\nu_{12}$=energy difference between states
N^+=number of electrons in upper state
N^-=number of electrons in lower state

Figure 1. Energy levels of a spin $\frac{1}{2}$ system.

If this system is subjected to a microwave field at frequency ν_{12}, the resulting equilibrium absorbtion of energy (ESR) can be written (assuming no saturation)[4] as:

$$A = n_{ss} \left| C_{-\frac{1}{2},\frac{1}{2}} \right|^2 h\nu_{12}\, g(\nu_{12}) \qquad (1\text{-}1)$$

where $C_{-\frac{1}{2},\frac{1}{2}}$ is the matrix element connecting the states, $g(\nu_{12})$ is a "shape function" due to the finite width of the energy levels, and n_{ss} is the steady state excess number of electrons in the ground state. Assuming Boltzmann population statistics (see Appendix I) we obtain:

$$n_{ss} = N \sinh\left[\frac{h\nu_{12}}{2kT}\right] \qquad (1\text{-}2)$$

where N is the total number of spins, k is Boltzmann's constant, and

T is the absolute temperature in ^{o}K. Examination of equation 1-2 reveals that the greatest population differences and hence the largest ESR signals are obtained at high magnetic fields and low temperatures.

B. The Wavefunctions of the Impurity States

Silicon has six conduction band minima in "k" space that lie along each of the directions $[1,0,0]$, $[-1,0,0]$, $[0,1,0]$, ..., $[0,0,-1]$ as shown in Figure 2.

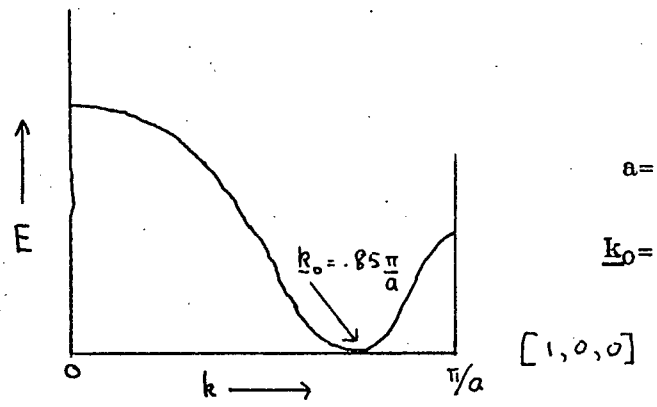

Figure 2. Energy vs $\underline{k}$ relationship in the $[1,0,0]$ direction.

The wavefunctions of the impurity states can be represented[5] by the following linear combination of the wavefunctions at each of these conduction band minima:

$$\Psi(\underline{r}) = F(\underline{r}) \sum_{n=1}^{6} \alpha_n e^{i\underline{k}_o^{(n)} \cdot \underline{r}} u_{\underline{k}_o^{(n)}}(\underline{r}) \qquad (1\text{-}3)$$

where α_n represents the contribution of each minimum to the total wavefunction, and $U_{\underline{K}_o^{(n)}}(\underline{r})$ is a periodic function of $\underline{r}$ corresponding to the n^{th} minimum. $F(\underline{r})$ is an envelope function satisfying a hydrogen-like Schroedinger equation:

$$\left[-\frac{\hbar^2}{2m_l}\frac{\partial^2}{\partial z^2} - \frac{\hbar^2}{2m_t}\left(\frac{\partial^2}{\partial x^2} + \frac{\partial^2}{\partial y^2}\right)\right] F(\underline{r}) - \frac{e^2}{Kr} F(\underline{r}) = E\, F(\underline{r}) \qquad (1\text{-}4)$$

where m_l is the longitudinal effective mass, m_t is the transverse

effective mass, e is the electronic charge and K is the macroscopic dielectric constant. Equation 1-4 is non-separable, but a good variational solution to it[6] is given by:

$$F(\underline{r}) = \frac{1}{\sqrt{\pi a^2 b}} e^{-\sqrt{\frac{x^2+y^2}{a^2} + \frac{z^2}{b^2}}} \qquad (1\text{-}5)$$

where a and b are, respectively, the transverse and longitudinal "effective Bohr radii".

As previously mentioned, this work will employ a single effective Bohr radius that enables equation 1-5 to be rewritten as:

$$F(\underline{r}) = \frac{1}{\sqrt{\pi a^{*3}}} e^{-\frac{r}{a^*}} \qquad (1\text{-}6)$$

where a^* is presumably some suitable average of a and b.

Kohn[5] finds, from considerations of symmetry and the experimentally observed ground state hyperfine splitting that $n = 1/\sqrt{6}$ for all n. Therefore we can write equation 1-3 for the ground state as:

$$\Psi(\underline{r}) = \frac{1}{\sqrt{6}} \cdot \frac{1}{\sqrt{\pi a^{*3}}} \cdot e^{-\frac{r}{a^*}} \sum_{n=1}^{6} e^{i\underline{k}_o^{(n)} \cdot \underline{r}} u_{\underline{k}_o^{(n)}}(\underline{r}) \qquad (1\text{-}7)$$

The interference term $e^{i\underline{k}_o(n)\cdot\underline{r}}$ in equation 1-7 will be retained explicitly in our further calculations.

C. The Nearest Donor Approximation

This study assumes a random distribution of the phosphorus impurities in the host lattice. This assumption has previously been shown to be reasonably justified in the concentration range of interest.[7] Further, we assume that the exchange interaction J between donor electrons is non-negligible for nearest neighbours only. Obviously, this approximation becomes inaccurate when some impurity site "A" is the same distance from neighbouring sites "B" and "C", but it is found that, for our concentration range, non-negligible probabilities of such clusters arise only when A, B and

C are so widely separated as to act like isolated donors. This approximation is also justified by the absence of lines due to such clusters in our spectra.

D. The Exchange Interaction

The nearest neighbour exchange interaction may be written as[8]:

$$V_{ex} = J\, \underline{S}_1 \cdot \underline{S}_2 \tag{1-8}$$

where $\underline{S1}$, $\underline{S2}$ are the spins of the two electrons concerned, and:

$$J = -\iint d\underline{r}_1\, d\underline{r}_2\, \frac{e^2}{r_{12}}\, \psi_1^*(\underline{r}_1)\, \psi_2^*(\underline{r}_2)\, \psi_1(\underline{r}_2)\, \psi_2(\underline{r}_1) - 2\iint \psi_1^*(\underline{r}_1)\, \psi_2(\underline{r}_1)\, d\underline{r}_1 \cdot \psi_1^*(\underline{r}_2)\left(-\frac{e^2}{r_{12}}\right)\psi_2(\underline{r}_2) \tag{1-9}$$

$$\equiv -J_{12}^{o} - 2 S_{12} L_{12} \tag{1-10}$$

where ψ_1, ψ_2 are the wavefunctions of electrons 1 and 2, and $r_{12} = |\underline{r}_1 - \underline{r}_2|$.

We can now calculate the exchange energy J as a function of interdonor separation $\underline{r}$ by substituting the impurity wavefunctions of equation 1-7 into equation 1-9. This is done in Appendix II, where we obtain:

$$\bar{J}(\underline{r}) = \frac{1}{9}\,\frac{e^2}{\kappa a^*}\left(\sum_n{}' \cos\left(\underline{k}_o^{(n)} \cdot \underline{r}\right)\right)^2 e^{-2D}\left\{2(1+D)\left(1+D+\frac{D^2}{3}\right) - \frac{1}{5}\left[-\left(-\frac{25}{8}+\frac{23D}{4}+3D^2+\frac{D^3}{3}\right)+\frac{6}{D}\left[\left(1+D+\frac{D^2}{3}\right)^2\left(\gamma+\ln D\right)\right]\right]\right\} \tag{1-11}$$

The $\left(\sum_n{}' \cos \underline{k}_o^{(n)} \cdot \underline{r}\right)^2$ factor represents an interference effect due to contributions from various conduction band minima.

E. The Donor Pair System

It is instructive to first calculate the donor pair spectrum in the two limiting cases of large (J≫A) and small (J≪A) exchange energy. The spin system is given in Figure 3.

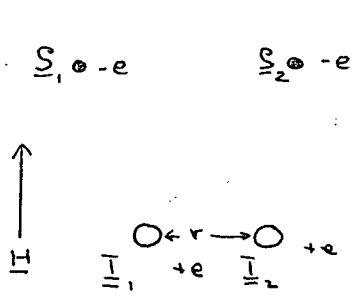

H = static magnetic field

I1, I2 are the individual nuclear spins

S1, S2 are the individual electronic spins of the pair

Figure 3. Spin system of the pair.

The Hamiltonian for this system can be written as:

$$\mathcal{H} = g\beta H\left[S_{1z} + S_{2z}\right] + A\left[\underline{I}_1 \cdot \underline{S}_1 + \underline{I}_2 \cdot \underline{S}_2\right] + J\,\underline{S}_1 \cdot \underline{S}_2 \qquad (1\text{-}12)$$

where g is the electronic g factor and β is the Bohr magneton. The much smaller nuclear Zeeman and nuclear spin-spin interactions are neglected. In the limit J≪A, the resulting spectra is obviously that of the isolated donor, which gives two hyperfine peaks at $E = g\beta H_0 \pm A/2$. The more interesting limit when J≫A shall now be considered in detail. For this situation $\underline{S} = \underline{S}_1 + \underline{S}_2$ is essentially a good quantum number. Neglecting the off-diagonal components of the hyperfine interaction, which is justified for almost all values of J (c.f. Chapter II, Section B), equation 1-12 becomes:

$$\mathcal{H} = g\beta H S_z + A S_z\left(\underline{I}_{1z} + \underline{I}_{2z}\right) + \tfrac{1}{2} J\left(S^2 - \tfrac{1}{2}\right) \qquad (1\text{-}13)$$

with eigenvalues:

$$E_T^{0,\pm 1} = g\beta H M + \tfrac{1}{2} A M (m_1 + m_2) + \frac{J}{4} \qquad (1\text{-}14)$$

and

$$E_S = -\frac{3}{4} J \qquad (1\text{-}15)$$

where E_T, E_S are the triplet and singlet energies (using the usual notation for the ground state of the hydrogen molecule). M is the total electronic spin projection quantum number, and m_1, m_2 are the individual nuclear spin projection numbers.

The introduction of a microwave field adds a perturbation to the Hamiltonian $\mathcal{H}$ of the form:

$$\mathcal{H}_{r.f.} = \frac{g\beta H_1}{2}(S^+ + S^-)\sin(\omega t) \qquad (1\text{-}16)$$

where S^+ is the electron spin raising operator, S^- is the electron spin lowering operator, and $\omega/2\pi$ is the frequency of transition. Clearly, this perturbation induces transitions such that $\Delta M = \pm 1$, $\Delta(m_1 + m_2) = 0$.

The transition $\Delta S = 1$ is not allowed. This is due to the fact that the spin wavefunctions of the triplet state are symmetric under interchange of electrons, whereas those of the ground state are antisymmetric under the same operation. Thus $\mathcal{H}_{r.f.}$, symmetric under this interchange, cannot connect the singlet to the triplet because of parity considerations. Note that when $J \sim A$, however, S is no longer a good quantum number and we observe[2] such "forbidden" transitions from the "singlet" to the "triplet" states.

From the selection rules given above, the ESR spectrum will have the form of Figure 4.

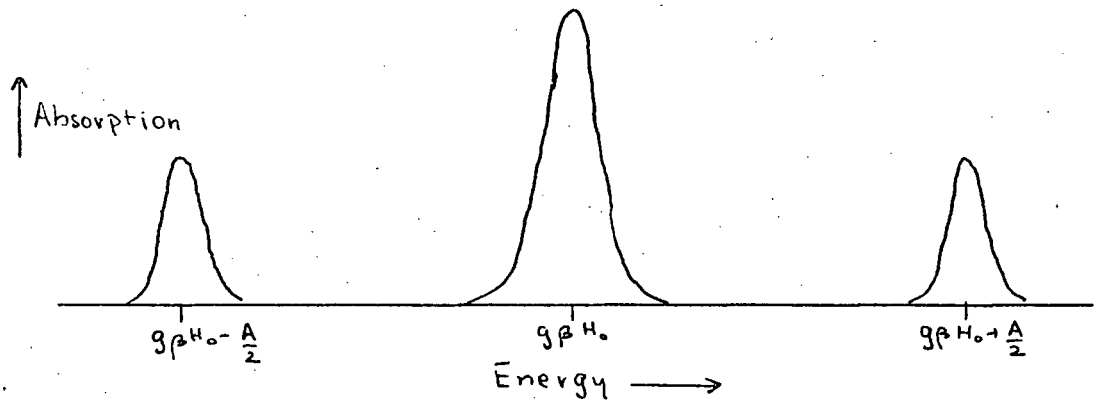

Figure 4. Spectrum of the pair system.

Note that the spectra due to the isolated donors will effectively mask the donor pair peaks at $E = g\beta H_0 \pm A/2$.

CHAPTER III

CALCULATION OF THE SPECTRUM

A. Introduction

The spectrum of P-SI is inhomogeneously broadened due to hyperfine interactions with Si^{29} nuclei (4%/o natural abundance). The following calculation will assume the existence of the "spin packets" proposed by Portis[9]. Each such spin packet constitutes a homogeneously broadened line corresponding to a particular effective local field, and has little interaction with those packets corresponding to different local fields. This is a questionable assumption and should be considered in more detail in future studies. For each of these packets the susceptibility $\chi = \chi' + i\chi''$ is given by[9]:

$$\chi'(H) = \frac{1}{2}\chi_0 \gamma^2 H_0 T_2^2 \frac{(H_0 - H)}{1 + T_2^2 \gamma^2 (H_0 - H)^2 + \gamma^2 H_1^2 T_1 T_2} \qquad (2\text{-}1)$$

$$\chi''(H) = \frac{1}{2}\chi_0 \gamma H_0 T_2 \frac{1}{1 + T_2^2 \gamma^2 (H_0 - H)^2 + \gamma^2 H_1^2 T_1 T_2} \qquad (2\text{-}2)$$

where χ_0 is the static magnetic susceptibility, γ is the free electron gyromagnetic ratio, H_1 is the microwave magnetic field intensity, T_1 and T_2 are the spin-lattice and spin-spin relaxation times respectively, and H_0 is the central resonant field of the spin packet.

Experimentally, we observe $d\chi'/dH$. Thus, realizing that for our low concentration samples ($<4\times10^{16}/cm^3$) $\gamma^2 H_1^2 T_1 T_2 \gg T_2^2 \gamma^2 (H-H_0)^2$ when $H \simeq H_0$, we obtain from equation 2-1 that:

$$\left(\frac{d\chi'(H)}{dH}\right)_{H \simeq H_0} \simeq \frac{\frac{1}{2}\chi_0 \gamma^2 H_0 T_2^2}{1 + \gamma^2 H_1^2 T_1 T_2} \qquad (2\text{-}3)$$

and thus from equation 2-2,

$$\left(\frac{d\chi'(H)}{dH}\right)_{H \simeq H_0} \simeq \gamma T_2 \chi''(H_0) \qquad (2\text{-}4)$$

Then, given that the rate of power absorbed by the sample is[9]:

$$A = 2\gamma H_0 \chi''(H_0) \tag{2-5}$$

we obtain from equations 1-1 and 2-4 that:

$$\left(\frac{d\chi'(H)}{dH}\right)_{H \cong H_0} \propto n_{ss} \left| C_{-\frac{1}{2},\frac{1}{2}} \right|^2 g(H - H_0) \tag{2-6}$$

where we assume a shape function $g(H-H_0)$ for the homogeneously broadened line of each spin packet to be of a Gaussian form. A theoretical calculation of a scale model of the spectrum therefore involves determining each of the terms on the right hand side of equation 2-6 over each interval of H corresponding to a spin packet width.

B. Matrix Element Calculations.

The calculation of the matrix elements of the allowed transitions necessitates a general calculation of the eigenvalues and eigenfunctions of the donor pair system over the whole range of J. Following the individual spin notation introduced in Figure 3, we can write the general form of the eigenfunctions as :

$$\psi^{(n)} = \sum_{i,j,k,l=1}^{2} C^{(n)}_{ijkl} \left| M_i M_j m_k m_l \right\rangle \tag{2-7}$$

where M_1, M_2 are the "z" components of the electronic spins $\underline{S}_1$ and $\underline{S}_2$, m_1 and m_2 are the "z" components of the nuclear spins $\underline{I}_1$ and $\underline{I}_2$, and the C_{ijkl}'s are normalized constants giving the contribution to the eigenfunction from each of the basis states.

There are 16 basic wavefunctions $\psi_{ijkl} = |M_i M_j m_k m_l\rangle$ and correspondingly 16 $C^{(n)}_{ijkl}$'s for a given $\psi^{(n)}$. The matrix representation of the Hamiltonian of the donor pair spin system (equation 1-12) in this basis is given in Table I. This matrix was diagonalized via computer and the corresponding eigenvalues and eigenfunctions determined for particular values of J. The eigenfunctions compiled in Table II have a particular form which guarantees that they be invariant under the

simultaneous interchange of both electron and nuclear spins (this operation commutes with the Hamiltonian given in equation 1-12.).

As this calculation of the eigenvectors and eigenvalues of for each value of J was tedious and costly in computer time, we determined their functional form by means of a hybrid method. Labelling the basis vectors Ψ_m by unprimed m,n 's, and the eigenvectors (in the diagonal representation) by m', n', we write

$$|m'\rangle = \sum_m' |m\rangle\langle m|m'\rangle = \sum_m' |m\rangle C_{mm'} \qquad (2\text{-}8)$$

where the Cmm' have already been calculated via computer for certain J's.

Then:

$$\mathcal{H}|m'\rangle = E_{m'}|m'\rangle = \sum_m' \mathcal{H}|m\rangle C_{mm'} \qquad (2\text{-}9)$$

or:

$$E_{m'}\langle n|m'\rangle = \sum_m' \langle n|\mathcal{H}|m\rangle C_{mm'} \qquad (2\text{-}10)$$

which we express more concisely as:

$$E_{m'} C_{nm'} = \sum_m' H_{nm} C_{mm'} \qquad (2\text{-}11)$$

In accord with equation 2-11 the n^{th} row of Hnm was multiplied by the column vector $|m'\rangle$ and the equation was solved for the corresponding Em'. This calculation was facilitated by neglecting the off-diagonal elements of the hyperfine interaction. A check on this approximation was made by comparing the eigenvalues projected by computer (in which the off-diagonal elements were not neglected) and the calculated Em' in the region J~A, with gratifying results (See Table III). The functional Em' 's are given in Table II and the energy level structure in Figure 5, where S, To, and T±1 refer to electronic pair spin states, and $s, t_0, t_{\pm 1}$ refer to similar

nuclear pair spin states, in the J≫A limit.

The non-zero values of the matrix elements connecting the various states under the influence of the microwave radiation are now easily calculated and are given in Table IV, together with the corresponding transition energy "Δ". Examination of Δ reveals the different regions of the spectrum to which each transition contributes. This is illustrated in Figure 6.

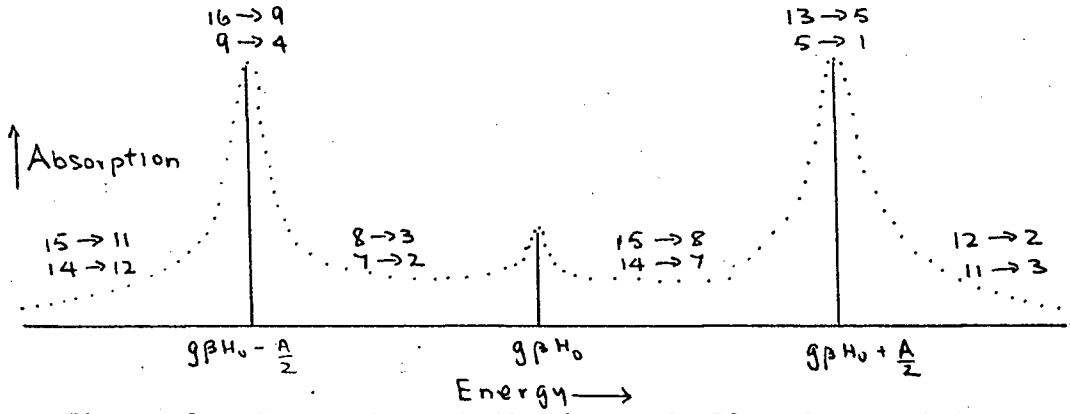

Figure 6. Spectral contributions of allowed transitions.

The broad background line is shown to be at least partly due to donor pairs for which J~A.

TABLE I

Matrix Representation of the Hamiltonian of the Donor Pair System

$\langle \frac{1}{2}\frac{1}{2}\frac{1}{2}\frac{1}{2}\|$	$\langle \frac{1}{2}\frac{1}{2}\frac{1}{2}-\frac{1}{2}\|$	$\langle \frac{1}{2}\frac{1}{2}-\frac{1}{2}\frac{1}{2}\|$	$\langle \frac{1}{2}\frac{1}{2}-\frac{1}{2}-\frac{1}{2}\|$	$\langle \frac{1}{2}-\frac{1}{2}\frac{1}{2}\frac{1}{2}\|$	$\langle \frac{1}{2}-\frac{1}{2}\frac{1}{2}-\frac{1}{2}\|$	$\langle \frac{1}{2}-\frac{1}{2}-\frac{1}{2}\frac{1}{2}\|$	$\langle \frac{1}{2}-\frac{1}{2}-\frac{1}{2}-\frac{1}{2}\|$	$\langle -\frac{1}{2}\frac{1}{2}\frac{1}{2}\frac{1}{2}\|$	$\langle -\frac{1}{2}\frac{1}{2}\frac{1}{2}-\frac{1}{2}\|$	$\langle -\frac{1}{2}\frac{1}{2}-\frac{1}{2}\frac{1}{2}\|$	$\langle -\frac{1}{2}\frac{1}{2}-\frac{1}{2}-\frac{1}{2}\|$	$\langle -\frac{1}{2}-\frac{1}{2}\frac{1}{2}\frac{1}{2}\|$	$\langle -\frac{1}{2}-\frac{1}{2}\frac{1}{2}-\frac{1}{2}\|$	$\langle -\frac{1}{2}-\frac{1}{2}-\frac{1}{2}\frac{1}{2}\|$	$\langle -\frac{1}{2}-\frac{1}{2}-\frac{1}{2}-\frac{1}{2}\|$
$\gamma H_0 + \frac{J}{4} + \frac{A}{2}$																
	$\gamma H_0 + \frac{J}{4}$			$\frac{A}{2}$												
		$\gamma H_0 + \frac{J}{4}$						$\frac{A}{2}$								
			$\gamma H_0 + \frac{J}{4} + \frac{A}{2}$			$\frac{A}{2}$			$\frac{A}{2}$							
	$\frac{A}{2}$			$-\frac{J}{4}$				$\frac{J}{2}$								
					$-\frac{J}{4} + \frac{A}{2}$				$\frac{J}{2}$							
			$\frac{A}{2}$			$-\frac{J}{4} - \frac{A}{2}$				$\frac{J}{2}$		$\frac{A}{2}$				
							$-\frac{J}{4}$				$\frac{J}{2}$		$\frac{A}{2}$			
		$\frac{A}{2}$		$\frac{J}{2}$				$-\frac{J}{4}$								
			$\frac{A}{2}$		$\frac{J}{2}$				$-\frac{J}{4} - \frac{A}{2}$				$\frac{A}{2}$			
						$\frac{J}{2}$				$-\frac{J}{4} + \frac{A}{2}$						
							$\frac{J}{2}$				$-\frac{J}{4}$			$\frac{A}{2}$		
						$\frac{A}{2}$			$\frac{A}{2}$				$-\gamma H_0 + \frac{J}{4} - \frac{A}{2}$			
							$\frac{A}{2}$							$-\gamma H_0 + \frac{J}{4}$		
											$\frac{A}{2}$				$-\gamma H_0 + \frac{J}{4}$	
																$-\gamma H_0 + \frac{J}{4} + \frac{A}{2}$

TABLE II

Eigenfunctions of the Donor Pair

State	$\vert\uparrow\uparrow\uparrow\uparrow\rangle$	$\vert\uparrow\uparrow\uparrow\downarrow\rangle$	$\vert\uparrow\uparrow\downarrow\uparrow\rangle$	$\vert\uparrow\uparrow\downarrow\downarrow\rangle$	$\vert\uparrow\downarrow\uparrow\uparrow\rangle$	$\vert\uparrow\downarrow\uparrow\downarrow\rangle$	$\vert\uparrow\downarrow\downarrow\uparrow\rangle$	$\vert\uparrow\downarrow\downarrow\downarrow\rangle$	$\vert\downarrow\uparrow\uparrow\uparrow\rangle$	$\vert\downarrow\uparrow\uparrow\downarrow\rangle$	$\vert\downarrow\uparrow\downarrow\uparrow\rangle$	$\vert\downarrow\uparrow\downarrow\downarrow\rangle$	$\vert\downarrow\downarrow\uparrow\uparrow\rangle$	$\vert\downarrow\downarrow\uparrow\downarrow\rangle$	$\vert\downarrow\downarrow\downarrow\uparrow\rangle$	$\vert\downarrow\downarrow\downarrow\downarrow\rangle$	Energy
1	1																$\gamma H_0 + \frac{J}{4} + \frac{A}{2}$
2		$1/\sqrt{2}$	$1/\sqrt{2}$														$\gamma H_0 + \frac{J}{4}$
3		$1/\sqrt{2}$	$-1/\sqrt{2}$														$\gamma H_0 + \frac{J}{4}$
4				1													$\gamma H_0 + \frac{J}{4} - \frac{A}{2}$
5					$1/\sqrt{2}$				$1/\sqrt{2}$								$\frac{J}{4}$
6					$-1/\sqrt{2}$				$1/\sqrt{2}$								$-\frac{3J}{4}$
7						a_1	a_2			a_2	a_1						$-\frac{J}{4} + \frac{1}{2}\sqrt{J^2+A^2}$
8						a_1	$-a_2$			a_2	$-a_1$						$-\frac{J}{4} + \frac{1}{2}\sqrt{J^2+A^2}$
9								$1/\sqrt{2}$				$1/\sqrt{2}$					$\frac{J}{4}$
10								$-\frac{1}{\sqrt{2}}$				$1/\sqrt{2}$					$-\frac{3J}{4}$
11						a_2	a_1			$-a_1$	$-a_2$						$-\frac{1}{2}\sqrt{J^2+A^2} + \frac{A}{2}$
12						a_2	$-a_1$			$-a_1$	a_2						$-\frac{1}{2}\sqrt{J^2+A^2} + \frac{A}{2}$
13													1				$-\gamma H_0 + \frac{J}{4} - \frac{A}{2}$
14														$1/\sqrt{2}$	$1/\sqrt{2}$		$-\gamma H_0 + \frac{J}{4}$
15														$-1/\sqrt{2}$	$1/\sqrt{2}$		$-\gamma H_0 + \frac{J}{4}$
16																1	$-\gamma H_0 + \frac{J}{4} + \frac{A}{2}$

TABLE III

A Comparison of (i) the Computer Projected Donor Pair Eigenvalues When the Off-diagonal Hyperfine Elements are not Neglected to (ii) the Functional Derivation Where These Off-diagonal Elements are Neglected.

State	J = 25 MHz		J = 400 MHz	
	(i)	(ii)	(i)	(ii)
1	10065.25	10065.25	10159.	10159.
2	10007.59	10006.25	10101.	10100.
3	10005.59	10006.25	10099.	10100.
4	9947.9	9947.25	10041.	10041.
5	6.59	6.25	99.7	100.
6	-18.39	-18.75	-299.6	-300.
7	54.06	54.06	108.5	108.5
8	54.06	54.06	108.5	108.5
9	5.9	6.25	100.3	100.
10	-22.46	-18.75	-300.3	-300.3
11	-66.56	-66.56	-308.5	-308.5
12	-66.56	-66.56	-308.5	-308.5
13	-10053.5	-10052.75	-9959.7	-9959.
14	-99941.1	-9993.75	-9900.	-9900.
15	-9994.1	-9993.75	-9900.	-9900.
16	-9934.75	-9934.75	-9841.	-9841.

TABLE IV

Donor Pair Transitions Having Non-zero Transition Probability. The Relative Transition Probabilities and the Transition Energies, Δ , are Given and $\nu_e = g\beta H_o$.

Transition	Relative Transition Probability	Transition Energy (Δ)
a: (16)↔(9)	1	$\nu_e - \frac{A}{2}$
b: (13)↔(5)	1	$\nu_e + \frac{A}{2}$
c: (9)↔(4)	1	$\nu_e - \frac{A}{2}$
d: (5)↔(1)	1	$\nu_e + \frac{A}{2}$
e: (15)↔(8)	$\frac{1}{2}(1 + J(J^2 + A^2)^{-\frac{1}{2}})$	$\nu_e + \frac{1}{2}(J^2 + A^2)^{\frac{1}{2}} - \frac{J}{2}$
f: (14)↔(7)	"	"
g: (8)↔(3)	"	$\nu_e - \frac{1}{2}(J^2 + A^2)^{\frac{1}{2}} + \frac{J}{2}$
h: (7)↔(2)	"	"
i: (15)↔(11)	$\frac{1}{2}(1 - J(J^2 + A^2)^{-\frac{1}{2}})$	"
j: (14)↔(12)	"	"
k: (12)↔(2)	"	$\nu_e + \frac{1}{2}(J^2 + A^2)^{\frac{1}{2}} + \frac{J}{2}$
l: (11)↔(3)	"	"

FIGURE 5

STATE NO.		STATE	ENERGY ($\gamma_e = g_\beta H$)
1	———	$\|T_1, t_1\rangle$	$\gamma_e + \frac{J}{4} + \frac{A}{2}$
2&3	———	$\|T_1, t_0\rangle, \|T, s\rangle$	$\gamma_e + \frac{J}{4}$
4	———	$\|T_1, t_{-1}\rangle$	$\gamma_e + \frac{J}{4} - \frac{A}{2}$
5&9	———	$\|T_0, t_1\rangle, \|T_0, t_{-1}\rangle$	$\frac{J}{4}$
7&8	———	$\|T_0, t_0\rangle, \|T_0, s\rangle$	$-\frac{J}{4} + \frac{1}{2}\sqrt{J^2+A^2}$
16	———	$\|T_{-1}, t_{-1}\rangle$	$-\gamma_e + \frac{J}{4} + \frac{A}{2}$
14&15	———	$\|T_{-1}, t_0\rangle, \|T, s\rangle$	$-\gamma_e + \frac{J}{4}$
13	———	$\|T_{-1}, t_1\rangle$	$-\gamma_e + \frac{J}{4} - \frac{A}{2}$
6&10	———	$\|S, t_1\rangle, \|S, t_{-1}\rangle$	$-\frac{3J}{4}$
11&12	———	$\|S, t_0\rangle, \|S, s\rangle$	$-\frac{J}{4} - \frac{1}{2}\sqrt{J^2+A^2}$

Energy Level Diagram for a Phosphorus Donor Pair. The Eigenstates are Labelled Numerically From 1 to 16 Along With the Usual Strongly Coupled Pair States to Which Each Reduces in the Limit $J \gg A$.

C. Calculation of the Population Difference Between Transition Levels

The population difference between the transition levels is given by n_{ss} as defined by equation 1-2. The determination of n_{ss} thus entails a knowledge of the relative number of pairs that contribute to a given spin packet, and also of the normalized distribution of spins in the corresponding upper and lower states at equilibrium. Appendix A deals with the latter calculation. As the transition energies Δ can be written in terms of J (Table IV), we shall calculate N(J), (the normalized distribution of nearest donor pairs having J values in a certain range) in order to find the relative number of pairs contributing to a given spin packet.

The nearest neighbour distribution function for a random distribution of impurities is given by Chandresklar[10] as:

$$W(r)\,dr = e^{-\frac{4\pi N_d r^3}{3}}\, 4\pi N_d r^2\, dr \qquad (2\text{-}12)$$

where N_d is the concentration of impurities and W(r)dr is the probability that the nearest neighbour to a given impurity lies in the spherical shell between r and r + dr. Noting that the factor $4\pi N_d r^3/3$ in equation 2-12 expresses the number of impurity sites inside a radius r, we write:

$$\frac{4\pi N_d r^3}{3} = \frac{N_d}{N_{sI}} \cdot n(r) \qquad (2\text{-}13)$$

where n(r) is the total number of lattice sites inside "r", and N_{sI} is the concentration of lattice sites. Similarly:

$$4\pi N_d r^2\, dr = \frac{N_d}{N_{sI}} \cdot n(r, r+dr) \qquad (2\text{-}14)$$

and therefore equation 2-12 can be rewritten as:

$$W(r)\,dr = \frac{N_d}{N_{sI}}\, n(r, r+dr)\, e^{-\frac{N_d}{N_{sI}} \cdot n(r)} \qquad (2\text{-}15)$$

The probability that any particular lattice site in the shell is

a nearest donor impurity site is then given by:

$$P(r) = \frac{N_d}{N_{SI}} \; e^{-\frac{N_d}{N_{SI}} \cdot n(r)} \qquad (2\text{-}16)$$

For particular values of N_d and a*, the determination of N(J) entails calculating J for each lattice site in a particular shell. Then, the probability that this lattice site is a nearest donor impurity site (as given by equation 2-16) is associated with this value of J. This analysis can then be performed over all possible shells, and the probabilities P(r) (whose J's fit into certain intervals) added in a corresponding array. Thus, for a particular concentration and effective Bohr radius, a discrete N(J) is determined. The computer analysis necessary to this computation is contained in Appendix C.

In order to make further calculation easier, a continuous N(J) was calculated by taking an appropriate average of the interference term in equation 1-11 (c.f. Appendix C). A comparison of the discrete and continuous distributions for $N_d = 4 \times 10^{16}/cm^3$ and $a^* = 16.5\text{Å}^o$ is given in Figure 7. (The rapid fall-off of the discrete curve in the region $\log J < -1$ is simply due to the fact that not all the pairs in this region were considered, due to limitations of computer time.)

The problem of determining the relative number of spins that contribute to a certain spin packet is now reduced to an integration of N(J) over the width of the packet expressed in terms of J. This is combined with the normalized Boltzmann population differences between the levels (Appendix A) to give Δn_{ss} of equation 2-6.

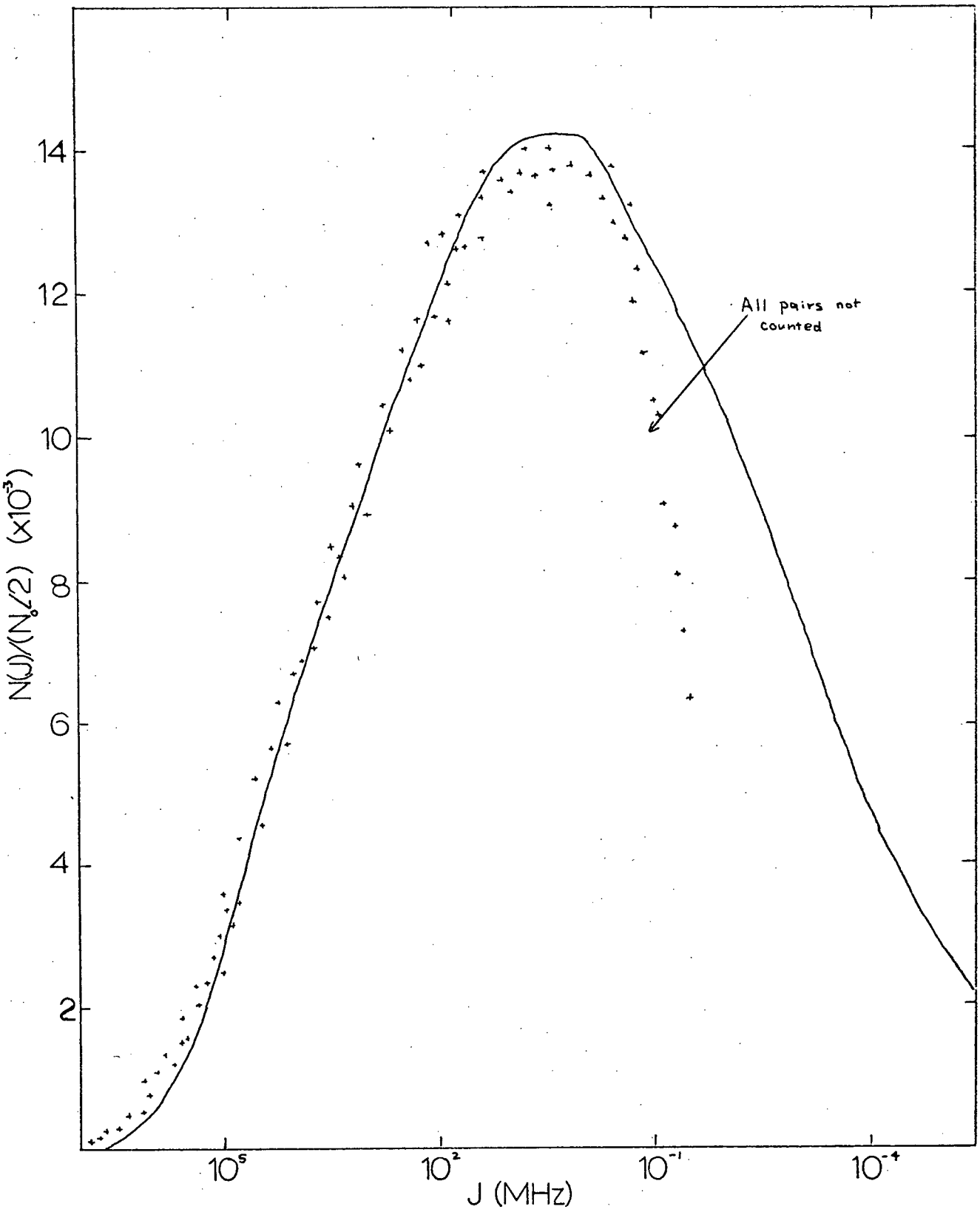

FIGURE 7

Comparison of Discrete and Continuous N(J)(a^*=16.5Å)

D. The Theoretical Spectrum

The final step in the calculation consists first of integrating the absorption A over one spin packet. We obtain $N_{J_1}^{J_2}$ where:

$$N_{J_1}^{J_2} = \int_{J_1}^{J_2} N(J) \cdot f_B(J,\Delta,T) \cdot M_{ij}^2(J)\, dJ \qquad (2\text{-}17)$$

where $E(J_1) - E(J_2)$ is the spin packet width, $f_B(J,\Delta,T)$ is the normalized Boltzmann population difference between the i and j levels, $M_{ij}^2(J)$ is the matrix element connecting the i and j states, and T is the temperature in ^{o}K. With reference to Figure 8, the Gaussian shape function is then introduced.

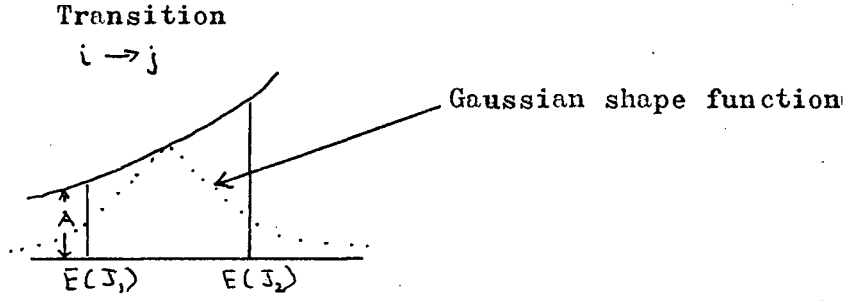

Figure 8. Introduction of the Gaussian shape function.

The total absorption $N_{J_1}^{J_2}$ is taken to be the area under the Gaussian shape function, with half width equal to the spin packet width (~ 8MHz). The convolution of all these contributing Ga ssians is then calculated and the resulting scaled spectrum is obtained. Appendix D presents the computer program that is used to perform these operations.

Subsequently, the ratio "C" of the height of the centre line to the average height of the hyperfine lines is calculated. This ratio is sensitive to the value of the "effective Bohr Radius" a*, and is particularly easy to determine experimentally.

CHAPTER IV

EXPERIMENTAL METHODS AND RESULTS

A. Apparatus and Operating Conditions

The gross features of the ESR spectrometer employed are seen in Figure 9. The klystron is a Varian Associates reflex type, delivering approximately 70 mW. over the frequency range 8.5 to 10GHz. The klystron frequency was stabilized by a standard automatic frequency control (AFC) that was "locked" to an external cavity of high Q and variable frequency, enabling observation in the dispersive mode. If we consider the equivalent circuit to a resonant cavity, χ' is proportional to the change in resonant frequency of the cavity as the resonant condition is swept through. It was found that the most sensitive position of the external cavity was approximately one half way up the resonant cavity as shown:

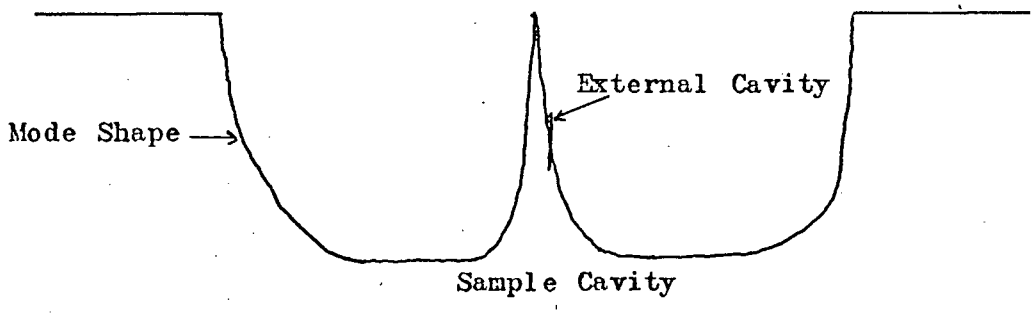

Figure 10. Mode shape and sample cavity.

where the change in reflected power (which is monitored by the crystal detector) per unit change in cavity frequency will presumably be maximum.

The brass cavity used was designed to operate in the TE_{102} mode and was gold plated by an immersion type gold plating solution. Aluminum foil wrapped around its exterior excluded any optical light,

and two pyrex filters situated in the waveguide just above the coupling hole shielded the sample from infra-red radiation[1]. Fairly consistent semi-critical coupling to the cavity was achieved as long as these filters were at least 1 cm. above the coupling hole. The samples used had dimensions $\sim$ 10 x 4 x 4 mm. and were held to the centre of the bottom of the cavity by vacuum grease.

Low temperatures were achieved by pumping on liquid He^4 that was transferred into an inner dewar containing the resonant cavity and waveguide. The pump used had a 150 cubic ft./min. capacity, and pumped on a 6" line. Temperatures achieved were found to be consistently close to $1.05^{o}K$ during the course of the experiments.

Field modulation coils that enabled observation of the derivative of the dispersion were operated at 400Hz and amplitude .5 Oersteds. The input to these coils also served as the reference for the lockin amplifier, to which was fed the output of the crystal preamplifier. The static magnetic field was provided by a Newport Instruments 8" electromagnet with variable sweep control.

FIGURE 9

Block Diagram of Experimental Apparatus

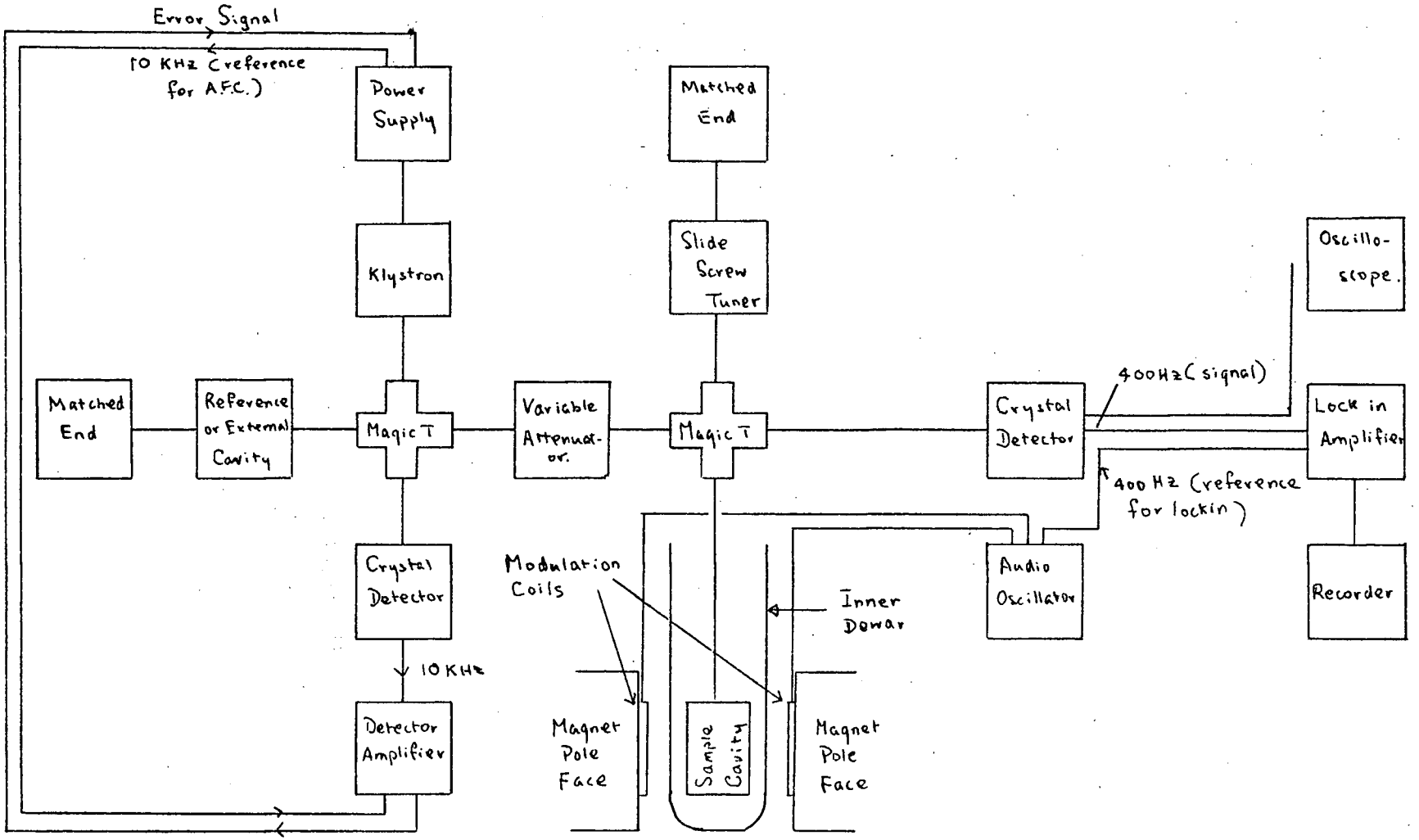

B. Experimental Results

The ESR spectrum was obtained at 1.05°K for four samples with concentrations of .8, 1.7, 2.3 and 3.7 x 10^{16} donors /cm^3. A typical spectra for Nd=4 x 10^{16} /cm^3 is shown in Figure 1. The experimental ration C of the centre line height to average hyperfine line height was plotted as seen in Figure 12. The theoretical ratio using an assumed effective Bohr radius a* was then calculated, and the best fit of the experimental results was obtained for a*=17.3A°. This theoretical ratio is seen as the solid line in Figure 12. Using this value of a* and the theoretical spectrum C was calculated to be 20.2 % for a Nd=3.7 x 10^{16} donors/cm^3 sample at 4.2°K. This is in good agreement with the experimental value of 20 $\pm$ 2%. Using this best fit value of a*=17.3A°, N(J) curves were then calculated for Nd=4 x 10^{16} /cm^3 and 6 x 10^{16} /cm^3, and are presented in Figure 13.

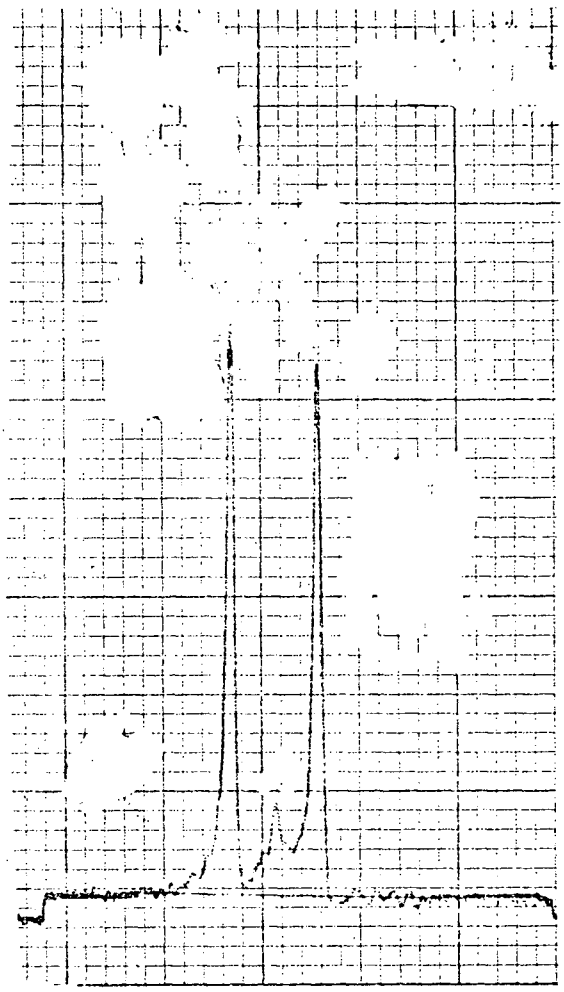

FIGURE 11

Experimental ESR Derivative Trace for $N_d = 3.7 \times 10^{16}/cm^3$

FIGURE 12

A Plot of Experimental Points and Theoretically Calculated Values of the Ratio C(%) of the Central Pair Line Intensity to the Average Intensity of the Hyperfine Lines. The Line Represents the Calculated Ratio for an Effective Bohr Radius $a^* = 17.3\text{A}^0$.

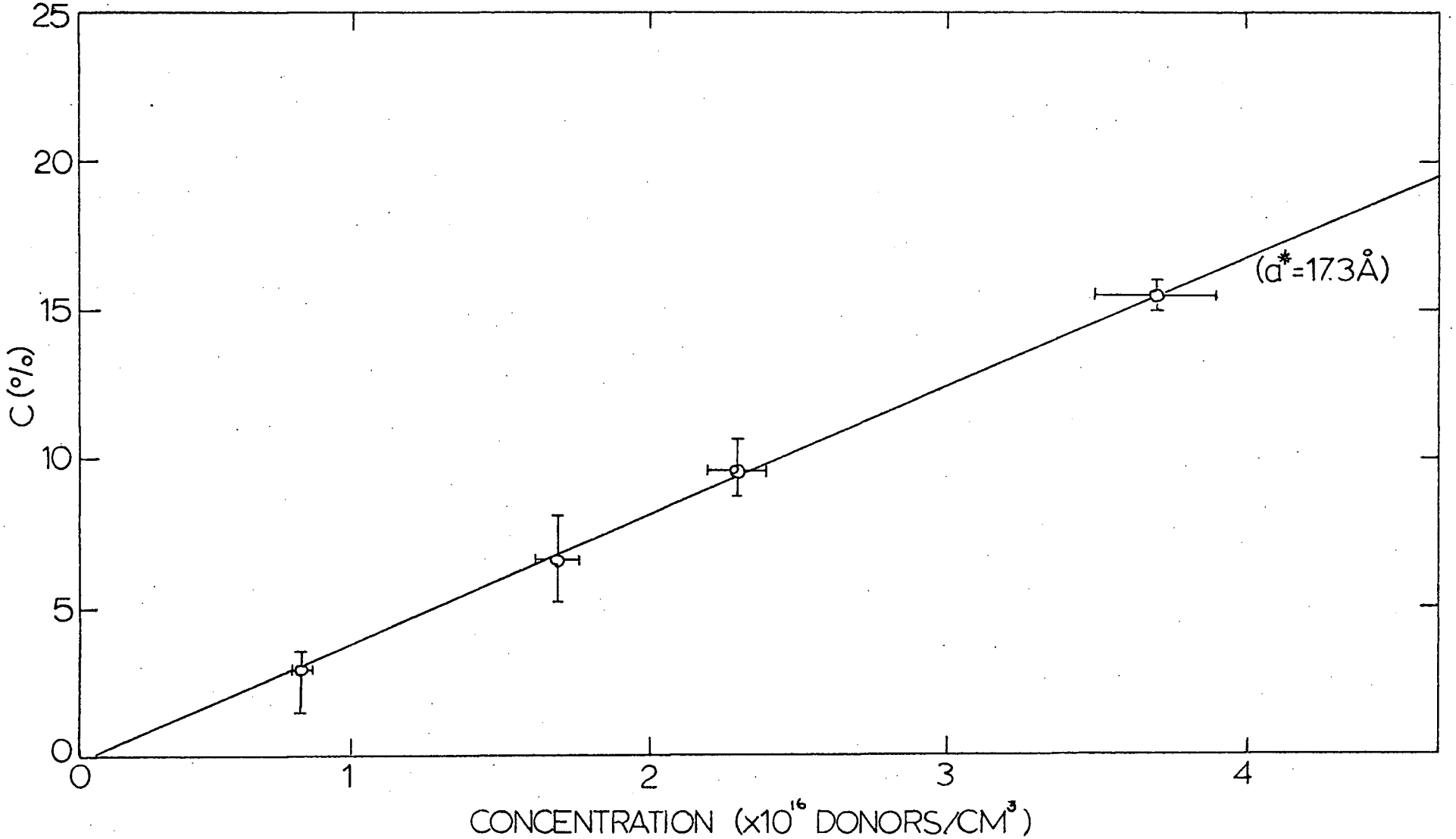

FIGURE 13

A Plot of the Normalized Distribution of Pair J Values N(J)/No/2 as a Function of the Exchange Energy J for a 4 x 10^{16} Donors /cm^3 Sample (Solid Curve) and a 6 x 10^{16} Donors /cm^3 Sample (Dashed Curve)

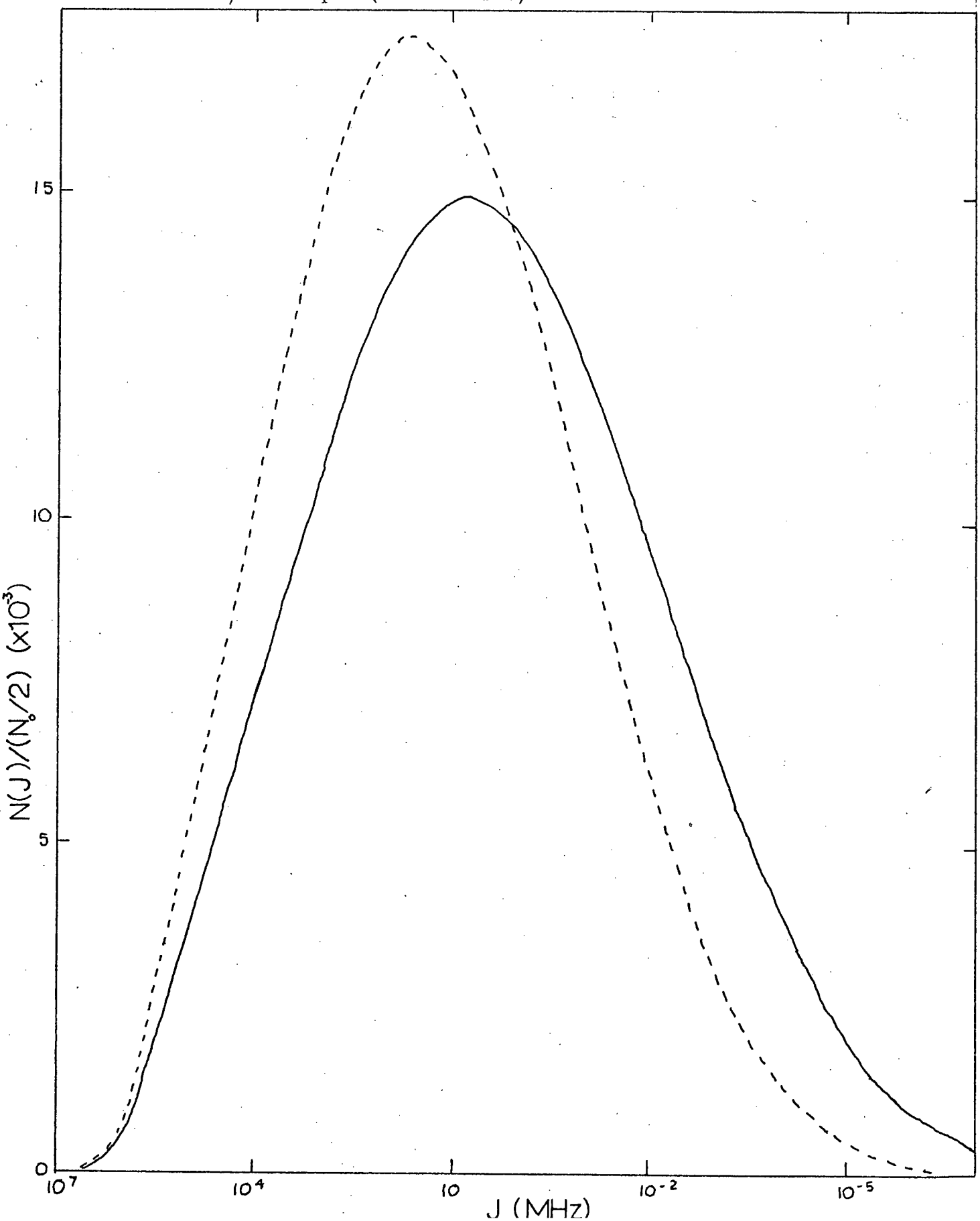

C. Possible Error

The measurement of the sample concentrations were made through a standard four point probe resistivity technique. These measurements had a possible error of $\pm$ 5%, which, together with possible experimental errors in measuring the ratio, are reflected by the error bars in Figure 12. Values of a* were then fitted to the limits of these error bars to define the accuracy of a*. We thus obtained $a^* = 17.3 A^o \pm .2 A^o$.

Additional errors may be due to a change in passage conditions from hyperfine to centre lines due to the more highly coupled and consequently faster relaxing pair systems that contribute to the centre line. We therefore changed several parameters of the observation mode, notably the sweep rate and magnetic field modulation frequency, which was varied from 30 Hz to 3000 Hz. Within experimental error the resulting values of the ratio were found to be independent of these changes in obervation parameters.

It was also found that the ratio "C" was significantly increased for higher microwave powers. This can be attributed to a spin diffusion phenomena[3] that would increase the faster relaxing centre line absorption at the expense of the more slowly relaxing hyperfine lines. To avoid such difficulties the ratio C was measured at the lowest microwave powers consistent with useable signal to noise.

CHAPTER V

DISCUSSION OF RESULTS

The experimentally determined effective Bohr radius $a^*=17.3A^o$ is very close to $17.2A^o$, which is the arithmetic mean of the longitudinal and transverse effective Bohr radii of the anisotropic ground state impurity wavefunction[12]. This agreement would seem to indicate that the effective Bohr radius in overlap calculations should be set equal to such an arithmetic mean rather than a geometric mean which has been used in previous calculations[13].

Jerome and Winter[14] via Endor techniques obtained the most probable value of J in a P-Si sample where $Nd=6 \times 10^{16}$ /cm^3 as 1.34×10^4 MHz. From Figure 13 which presents our normalized N(J) for a similar sample, the most probable value of J is seen to be 50 MH . Part of this discrepancy may be due to the complications introduced into the interpretation of Endor results due to the J dependent electronic spin lattice relaxation time. But more importantly, it might be pointed out that Endor measurements only involved those parts for which $J \geq A$, thus ignoring the great bulk of more weakly coupled pairs.

In conclusion, the excellent agreement that is achieved between the calculated and experimental results (Figure 13) provides confidence in the isotropic assumption of the effective Bohr radius, and also in our assumption of a random distribution of impurities. This unified, self consistent approach should provide useful and detailed information on the distribution of exchange coupled pairs which has hitherto been unavailable.

BIBLIOGRAPHY

1. Slichter, C.P., Phys. Rev. 99, 479 (1955)
2. Marko, J.R., Phys. Lett. 27A, 119 (1968)
3. Yang, G. and Honig, A., Phys. Rev. 168, 271 (1967)
4. Pake, G.E., Paramagnetic Resonance, Ed. D. Pines, 38 (W.A. Benjamin Inc., N.Y., 1962)
5. Kohn, W., in Solid State Physics, edited by F. Seitz and D. Turnbull (Academic Press Inc., N.Y., 1957), Vol. 5.
6. Kohn, W. and Luttinger, J.M., Phys. Rev. 98, 915 (1955)
7. Alexander, M.N. and Holcomb, D.F., Rev. Mod. Phys. 40, 815 (1968)
8. Anderson, P.W., in Solid State Physics, edited by F. Seitz and D. Turnbull (Academic Press Inc., N.Y., 1963), Vol. 14
9. Portis, A.M., Phys. Rev. 91, 1071 (1953)
10. Chandrasekhar, S., Rev. Mod. Phys. 15, 1 (1943)
11. Honig, A., Physica 24, 1635 (1958)
12. Miller, A. and Abrahams, E., Phys. Rev. 120, 745 (1960)
13. Sugihara, K., J. Phys. Chem. Solids 29, 1099 (1968)
14. Jerome, D. and Winter, J.M., Phys. Rev. 134, A1001 (1964)
15. Pauling, L. and Wilson, E.B., Introduction to Quantum Mechanics, 343 (McGraw-Hill Book Company Inc., N.Y., 1935)

APPENDIX A

POPULATION DIFFERENCES BETWEEN TRANSITION LEVELS

Our whole calculation of the spectrum is based on the fact that all the localized impurity pairs are "distinguishable". Therefore, even though the electrons are fermions, the relative populations of the various pair levels will be given by Boltzmann statistics. With reference to Figure 5, page 17, we discount the splitting of the various triplet lines (as $A \ll \gamma H_0$) and obtain the simplified energy level diagram given in Figure 15.

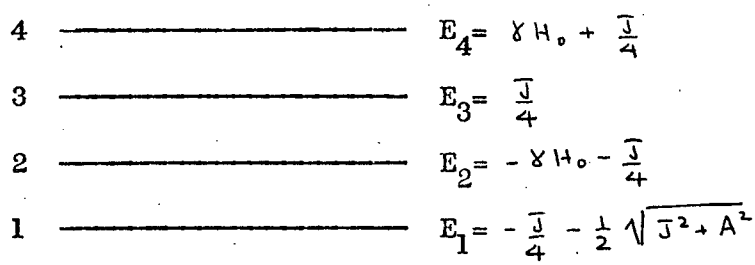

Figure 15. Simplified energy level diagram of the donor pair.

Therefore, if we assign a population of 1 to energy level 1, and a total population of N to the whole system, the fractional populations of the other states are given by:

State 1. $$N_1 = \frac{N e^{-\beta E_1}}{\sum_{\nu=1}^{4} e^{-\beta E_\nu}} \equiv 1 \qquad \text{(A-1-1)}$$

thus: $$\sum_{\nu=1}^{4} e^{-\beta E_\nu} = N e^{-\beta E_1} \qquad \text{(A-1-2)}$$

State 2. $$N_2 = \frac{N e^{-\beta E_2}}{\sum_{\nu=1}^{4} e^{-\beta E_\nu}} = e^{\beta(E_1 - E_2)} \qquad \text{(A-1-3)}$$

and similarly for states 3 and 4. The results of this calculation and corresponding population differences are given in Table V.

TABLE V

Boltzmann Population Differences Between Transition Levels

Transition	Population Difference $f_B(J, \Delta, T)$
15 → 8 14 → 7	$\exp\left[-\frac{(J+\sqrt{J^2+A^2})}{2kT}\right]\left\{\exp\left[\frac{\gamma H_0}{kT}\right]-1\right\}$
7 → 2 8 → 3	$\exp\left[-\frac{(J+\sqrt{J^2+A^2})}{2kT}\right]\left\{1-\exp\left[-\frac{\gamma H_0}{kT}\right]\right\}$
11 → 15 12 → 14	$\left\lvert\left(1-\exp\left[\frac{2\gamma H_0 - J - \sqrt{J^2+A^2}}{2kT}\right]\right)\right\rvert$
12 → 2 11 ↪ 3	$1-\exp\left[-\frac{(2\gamma H_0 + J + \sqrt{J^2+A^2})}{2kT}\right]$
16 → 9 13 → 5	$\exp\left[-\frac{(J+\sqrt{J^2+A^2})}{2kT}\right]\left\{\exp\left[\frac{\gamma H_0}{kT}\right]-1\right\}$

APPENDIX B

CALCULATION OF EXCHANGE

The term J°_{12} of equation 1-10 is now to be calculated explicitly.

Substituting the shielded potential $-e^2/\kappa r_{12}$ seen by the donor electrons for the hydrogenic potential $-e^2/r_{12}$, and writing $\underline{r}=\underline{r}_2-\underline{r}_1$ we obtain:

$$J^{\circ}_{12} = \frac{e^2}{\kappa}\int \psi_1^*(\underline{r}_1-\underline{r})\,\psi_2(\underline{r}_2)\left\{\int \psi_2^*(\underline{r}_1+\underline{r})\,\psi_2(\underline{r}_1)\,d\underline{r}_1\right\}d\underline{r}_2 \qquad \text{(A-2-1)}$$

As

$$\psi_1(\underline{r}) = F(\underline{r})\sum_n \alpha_n e^{i\underline{k}_o^{(n)}\cdot\underline{r}}\,u_{\underline{k}_o^{(n)}}(\underline{r}) \quad ,$$

J°_{12} can now be written:

$$J^{\circ}_{12} = \frac{e^2}{\kappa}\int F_1(\underline{r}_2-\underline{r})\,F_2(\underline{r}_2)\sum_{n,n'}\alpha_n\alpha_{n'}\,e^{-i\underline{k}_o^{(n)}\cdot(\underline{r}_2-\underline{r})}e^{i\underline{k}_o^{(n')}\cdot\underline{r}_2}\,u_{\underline{k}_o^{(n)}}(\underline{r}_2-\underline{r})\,u_{\underline{k}_o^{(n)}}(\underline{r}_2)$$
$$\cdot\left\{\int \frac{F_2(\underline{r}_1+\underline{r})\,F_1(\underline{r}_1)}{r}\sum_{n'',n'''}\alpha_{n''}\alpha_{n'''}\,e^{-i\underline{k}_o^{(n'')}\cdot(\underline{r}_1+\underline{r})}e^{i\underline{k}_o^{(n''')}\cdot\underline{r}_1}\,u_{\underline{k}_o^{(n'')}}(\underline{r}_1+\underline{r})\,u_{\underline{k}_o^{(n''')}}(\underline{r}_1)\,d\underline{r}_1\right\}d\underline{r}_2 \qquad \text{(A-2-2)}$$

We examine the inner integral given by $\{\ \}$. Using the periodicity of the u's ($u_{\underline{k}_o^{(n''')}}(\underline{r}_1+\underline{r}) = u_{\underline{k}_o^{(n''')}}(\underline{r})$)

$$\{\ \} = \sum_{n'',n'''}\alpha_{n''}\alpha_{n'''}\,e^{-i\underline{k}_o^{(n'')}\cdot\underline{r}}\int \frac{F_2(\underline{r}_1+\underline{r})\,F_1(\underline{r}_1)}{r}e^{i\left(\underline{k}_o^{(n''')}-\underline{k}_o^{(n'')}\right)\cdot\underline{r}_1}\,u_{\underline{k}_o^{(n'')}}(\underline{r}_1)\cdot u_{\underline{k}_o^{(n''')}}(\underline{r}_1)\,d\underline{r}_1 \qquad \text{(A-2-3)}$$

As $u_{\underline{k}_o^{(n'')}}(\underline{r}_1)\,u_{\underline{k}_o^{(n''')}}(\underline{r}_1)$ is periodic in $\underline{r}_1$, we expand it in a Fourier series:

$$u_{\underline{k}_o^{(n'')}}(\underline{r}_1)\,u_{\underline{k}_o^{(n''')}}(\underline{r}_1) = \sum_{\underline{\nu}} B^{\underline{\nu}}_{n''n'''}\,e^{-i\underline{K}_{\underline{\nu}}\cdot\underline{r}_1} \qquad \text{(A-2-4)}$$

Thus:

$$\{\ \} = \sum_{n'',n'''}\alpha_{n''}\alpha_{n'''}\,e^{-i\underline{k}_o^{(n'')}\cdot\underline{r}}\left(\sum_{\underline{\nu}} B^{\underline{\nu}}_{n''n'''}\int \frac{F_2(\underline{r}_1+\underline{r})\,F_1(\underline{r}_1)}{r}e^{i\left(\underline{k}_o^{(n''')}-\underline{k}_o^{(n'')}-\underline{K}_{\underline{\nu}}\right)\cdot\underline{r}_1}\,d\underline{r}_1\right) \qquad \text{(A-2-5)}$$

Then, if $U = \frac{F_2(\underline{r}_1+\underline{r})\,F_1(\underline{r}_1)}{r}$ varies slowly with $\underline{r}_1$, (this is

equivalent to the "gentle potential approximation[5]" basic to the derivation of the impurity wavefunctions) one can obtain:

$$\int U\, e^{i\left(\underline{k}_0^{(n''')} - \underline{k}_0^{(n'')} - \underline{K}_\gamma\right)\cdot \underline{r}_1} \xrightarrow[\left(\text{limit } \frac{\partial U}{\partial r_1} \to 0\right)]{} (\text{Const})\, \delta\left|\underline{k}_0^{(n''')} - \underline{k}_0^{(n'')} - \underline{K}_\gamma\right| \quad \text{(A-2-6)}$$

by using the common definition of the delta function.

As $\underline{k}_0^{(n''')}$ and $\underline{k}_0^{(n'')}$ are both in the first Brillouin zone, and $\underline{K}_\gamma$ is a reciprocal lattice vector, equation A-2-6 demands $\underline{K}_\gamma = 0$ or $\gamma = 0$ for non-negligible contributions in this gentle potential limit. Similarly, $\underline{k}_0^{(n''')}$ and $\underline{k}_0^{(n')}$ must be in the same direction in order that their difference be close to zero, which provides the condition $n''' = n''$. Therefore

$$\left\{\ \right\} = \sum_{n''}^{1} \alpha_{n''}^2\, e^{-i\underline{k}_0^{(n'')}\cdot \underline{r}} \int \frac{F_2(\underline{r}_1 + \underline{r})\, F_1(\underline{r}_1)}{r}\, d\underline{r}_1 \quad \text{(A-2-7)}$$

where the orthonormality of the $u_{\underline{k}_0^{(n)}}(\underline{r})$'s has been used to obtain $\beta^0_{n'',n'''} = 1$.

Thus

$$J_{12}^0 = \sum_{n''}^{1} \alpha_{n''}^2\, e^{-i\underline{k}_0^{(n'')}\cdot \underline{r}} \iint \frac{F_1(\underline{r}_2 - \underline{r})\, F_2(\underline{r}_2)\, F_2(\underline{r}_1 + \underline{r})\, F_1(\underline{r}_1)}{r} \cdot \sum_{n,n'}^{1} \alpha_n \alpha_{n'}\, e^{i\underline{k}_0^{(n)}\cdot \underline{r}}\, e^{i\left(\underline{k}_0^{(n')} - \underline{k}_0^{(n)}\right)\cdot \underline{r}_1}\, u_{\underline{k}_0^{(n)}}(\underline{r}_1)\, u_{\underline{k}_0^{(n')}}(\underline{r}_1)\, d\underline{r}_1\, d\underline{r}_2 \quad \text{(A-2-8)}$$

which, by the same type of procedure can be written as

$$J_{12}^0 = \sum_{n,n'}^{1} \frac{\alpha_n^2\, \alpha_{n'}^2}{K}\, e^{i\left(\underline{k}_0^{(n)} - \underline{k}_0^{(n')}\right)\cdot \underline{r}} \cdot \overbrace{e^2 \iint \frac{F_1(\underline{r}_1)\, F_2(\underline{r}_2)\, F_1(\underline{r}_2)\, F_2(\underline{r}_1)\, d\underline{r}_2\, d\underline{r}_1}{r}}^{K} \quad \text{(A-2-9)}$$

Noting that the F_1's, F_2's are hydrogenic 1s wavefunctions with an effective Bohr radius a*, the integral K is regognized to be equivalent to the integral K' evaluated by Pauling and Wilson[15] in a treatment of the hydrogen molecule, where a = a*. They obtain

$$K = \frac{e^2}{a^*}\left[-e^{-2D}\left(-\frac{25}{8}+\frac{23}{4}D+3D^2+\frac{1}{3}D^3\right)+\frac{6}{D}\left\{\Delta^2(\gamma+\ln D)\right.\right.$$
$$\left.\left.+\Delta'^2 E_i(-4D)-2\Delta\Delta' E_i(-2D)\right\}\right] \qquad \text{(A-2-10)}$$

where $D = r/a^*$

$\gamma = .57722$

$\Delta = e^{-D}(1+D+D^2/3)$

By an exactly similar analysis, using 42-10, 42-12 of Pauling and Wilson[15]:

$$S_{12} = \sum_n^1 \alpha_n^2 e^{i\underline{k}_o^{(n)}\cdot\underline{r}}\,\Delta \qquad \text{(A-2-11)}$$

and

$$L_{12} = \sum_{n'}^1 \alpha_{n'}^2 e^{-i\underline{k}_o^{(n')}\cdot\underline{r}}\left(-\frac{e^2}{K}\right)e^{-D}(1+D) \qquad \text{(A-2-12)}$$

As $J_{12} = J_{12}^o - 2S_{12}L_{12}$, we have as our final expression:

$$J_{12} = \frac{e^2}{Ka^*}\sum_{n,n'}^1 \alpha_n^2\alpha_{n'}^2 e^{i(\underline{k}_o^{(n)}-\underline{k}_o^{(n')})\cdot\underline{r}}e^{-2D}\left\{2(1+D)(1+D+\frac{D^2}{3})\right.$$
$$\left.-\frac{1}{5}\left\{-\left(-\frac{25}{8}+\frac{23}{4}D+3D^2+\frac{1}{3}D^3\right)+\frac{6}{D}\left[\left(1+D+\frac{D^2}{3}\right)^2(\gamma+\ln D)\right]\right\}\right\} \qquad \text{(A-2-13)}$$

where terms $O(E_i(-2D))$ have been discounted as they go to zero very quickly for $D \gtrsim \frac{1}{2}$.

As $|\underline{k}_o^{(n)}| = .85\,\pi/a$, where a is the lattice spacing, for all n, the interference term in equation A-2-13 can be rewritten as:

$$\sum_{n,n'}^1 \alpha_n\alpha_{n'} e^{i(\underline{k}_o^{(n)}-\underline{k}_o^{(n')})\cdot\underline{r}} = 4\left(\sum_n^1 \cos(\underline{k}_o^{(n)}\cdot\underline{r})\right)^2 \qquad \text{(A-2-14)}$$

Therefore, equation A-2-13 becomes:

$$\bar{J}_{12}(r) = \frac{1}{9}\cdot\frac{e^2}{\kappa a^*}\cdot\left(\sum_n \cos\left(\underline{k}_o^{(n)}\cdot\underline{r}\right)\right)^2 e^{-2D}\left\{2(1+D)\left(1+D+\frac{D^2}{3}\right)\right.$$
$$\left.-\frac{1}{5}\left[-\left(-\frac{25}{8}+\frac{23}{4}D+3D^2+\frac{1}{3}D^3\right)+\frac{6}{D}\left[\left(1+D+\frac{D^2}{3}\right)^2\left(\gamma+\ln D\right)\right]\right]\right\} \quad \text{(A-2-15)}$$

which is our final expression.

APPENDIX C

THE DISTRIBUTION OF NEAREST EXCHANGE COUPLED PAIRS

a. Calculation of the Number of Lattice Sites in Shells of Unit Thickness Centered on the Origin.

Silicon has a so-called "diamond" crystalline structure consisting of two interlocking face-centred cubic lattices.

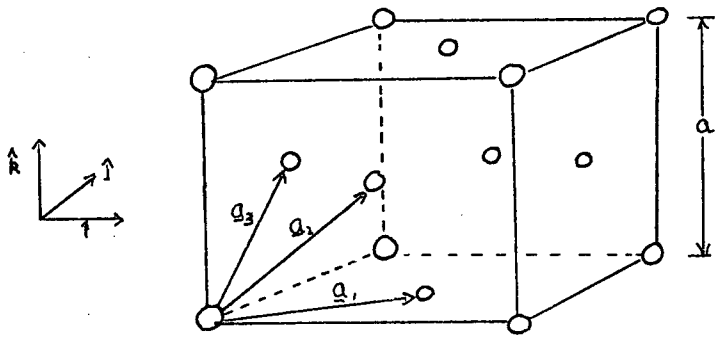

Figure 14. Simple Face-centred Cubic Lattice Structure (F.C.C.)

For the simple F.C.C. lattice noted in the above figure, the basic lattice transformations depicted are given by

$$\underline{a}_1 = \frac{a}{2}(\hat{i} + \hat{j})$$
$$\underline{a}_2 = \frac{a}{2}(\hat{i} + \hat{j}) \qquad \text{(A-3-1)}$$
$$\underline{a}_3 = \frac{a}{2}(\hat{j} + \hat{k})$$

Therefore, lattice sites are at positions $\underline{R}$ where

$$\underline{R} = n_1\underline{a}_1 + n_2\underline{a}_2 + n_3\underline{a}_3 \text{ where } n_1, n_2, n_3 \text{ are integers.} \qquad \text{(A-3-2)}$$

The second F.C.C. lattice of silicon is displaced along the body diagonal of the cube depicted in Figure 14 by $\frac{1}{4}$ of its length. Therefore the lattice points of the second lattice are described by

$\underline{R}$ where:

$$\underline{R}' = \underline{R} + \frac{a}{4}\left(\hat{i} + \hat{j} + \hat{k}\right) \qquad \text{(A-3-3)}$$

The distance $R = \left(\underline{R}\cdot\underline{R}\right)^{\frac{1}{2}}$ of the lattice sites from the origin is then given by:

$$R = \frac{a}{2}\sqrt{(n_1+n_2)^2 + (n_1+n_3)^2 + (n_2+n_3)^2} \qquad \text{(A-3-4)}$$

for the first lattice, and by:

$$R' = \frac{a}{2}\sqrt{(n_1+n_2+.5)^2 + (n_1+n_3+.5)^2 + (n_2+n_3+.5)^2} \qquad \text{(A-3-5)}$$

for the second lattice.

When this formulation is used in the 360-67 computer to calculate the number of lattice sites in shells of width 1 Å, it becomes extremely costly in computer time to proceed past r= 100 Å. It is, however, essential to the calculation that we do so. Thus the problem was reformulated by using the symmetry properties of the lattice.

The basic quantities of interest are the absolute value of $\underline{R}$ and (for the interference term in eq. A-2-15) the projections of $\underline{R}$ on the x, y, z axes respectively. The interference term is seen to be an even function of these projections. Therefore we shall calculate the absolute value of the projections of various $\underline{R}$ on the x, y, z axes respectively and find the number of lattice sites that correspond to each set of projections. The analysis, although tedious, is conceptually trivial, and in essence consists of treating the two interlocking F.C.C. lattices as 8 interlocking cubic lattices. The resulting absolute values of the projections and corresponding lattice sites are summarized in Table VI. It was then easy to calculate the number of lattice sites contained in each shell of width 1 Å, and to subsequently obtain the probability that any one site in that shell was an impurity site through equation 2-16.

TABLE VI

Number of Lattice Sites Having the Same Absolute Value for Projections on the x, y, z Axes in a Crystal With Interlocking F.C.C. Structure.

Absolute Value of Projections (n_1, n_2, $n_3 \geq 1$ where n_1, n_2, n_3 are integers)			No. of "Equivalent" Sites
x	y	z	
$n_1 a$	$(n_2 - 1)a$	$n_3 a$	8
$n_1 a$	$(n_2 - .5)a$	$(n_3 - .5)a$	24
$(n_1 - .75)a$	$(n_2 - .75)a$	$(n_3 - .25)a$	12
$(n_1 - .75)a$	$(n_2 - .25)a$	$(n_3 - .25)a$	12
$(n_1 - .75)a$	$(n_2 - .75)a$	$(n_3 - .75)a$	4
$(n_1 - .25)a$	$(n_2 - .25)a$	$(n_3 - .25)a$	4
$(n_1 - .5)a$	$(n_2 - .5)a$	0	12
$n_1 a$	$n_2 a$	0	4
$n_1 a$	0	0	6

b. Determination of the Nearest Neighbour Distribution

This was performed by Program I. The probability that a lattice site in a particular shell was a nearest donor, as calculated in Section A for a particular concentration Nd, was read in as the array P. The exchange energy J was then calculated, according to equation 1-10, for each collection of "equivalent" sites assuming an effective Bohr radius a* (=AD). Subsequently, depending upon which range the log(J) term corresponds to, the probability P multiplied by the number of equivalent sites L is added to a certain element of the FTϕT array. This program is run for all the equivalent sites noted in Table VI, which entails nine separate computations in order to obtain the final discrete FTϕT , or N(J), array.

PROGRAM I

```
$LIS THENOJ
      1              DIMENSION RR(250),NO(250),PROB(250),ALJ(250),P(250),FTOT(250
      2              REAL LGE,JJ(250)
      3              AA=2.90E08
      4              BB=2./9.
      5              CC=1./45.
      6              ALPHA=5.3
      7              E=.85*3.1416
      8              LGE=ALOG10(2.71828)
      9              READ (4,100) DIST,AD
     10      100     FORMAT (2F10.2)
     11              N=DIST
     12              DO 2 I=1,N
     13              READ (5,101) RR(I),NO(I),P(I)
     14      101     FORMAT (F10.2,I10,E10.2)
     15              NO(I)=0
     16              FTOT(I)=0.
     17              PROB(I)=0.
     18      2       CONTINUE
     19              M=INT(DIST/5.3)
     20              NJMAX=90
     21              NJMIN=-15
     22              NN=NJMAX+16
     23              READ (4,104) GOD
     24      104     FORMAT (F10.2)
     25              IF (GOD.EQ.0.) GO TO 8
     26              DO 6 I=1,NN
     27              READ (3,102) JJ(I),JJ(I+1),ALJ(I),ALJ(I+1),PROB(I)
     28      6       CONTINUE
     29              DO 7 I=1,N
     30              READ (3,103) RR(I),NO(I),FTOT(I)
     31      7        CONTINUE
     32      8       CONTINUE
     33              DO 1 I=1,M
     34                .
     35
     36              A=I
     37              B=0
     38              C=0
     39              L=6
     40              R=ALPHA*SQRT(A**2+B**2+C**2)
     41              IF (R.GT.DIST+1) GO TO 1
     42              NR=R
     43              F=(COS(E*A)+COS(E*B)+COS(E*C))**2
     44              FTOT(NR)=FTOT(NR)+ALOG10(F)*L
     45              NO(NR)=NO(NR)+L
     46              D=R/AD
     47              FD=AA*BB*(1.+D)*(1.+D+D**2/3.)*EXP(-2.*D)/AD
     48              GD=AA*CC*(25./8.-5.75*D-3.*D**2-D**3/3.
     49             2+(6./D)*((1.+D+D**2/3.)**2)*(.57777+ALOG(D)))*EXP(-2.*D)/AD
     50              X=F*(FD-GD)
     51                .
     52              NJ=INT(10.*ALOG10(X))
```

```
    53              IF (NJ.LT.NJMIN) GO TO 1
    54              NJ=NJ+16
    55              PROB(NJ)=PROB(NJ)+L*P(NR)
    56        1     CONTINUE
    57              ALJ(1)=-15
    58              JJ(1)=EXP(ALJ(1)/(10.*LGE))
    59              ALJ(1)=-1.5
    60              DO 4 I=1,NN
    61              ALJ(I+1)=(I-15)/10.
    62              JJ(I+1)=EXP(ALJ(I+1)/LGE)
    63              WRITE (6,102) JJ(I),JJ(I+1),ALJ(I),ALJ(I+1),PROB(I)
    64              WRITE (7,102) JJ(I),JJ(I+1),ALJ(I),ALJ(I+1),PROB(I)
    65        4     CONTINUE
    66        102   FORMAT (2E10.2,2F10.2,1PE10.2)
    67              DO 5 I=1,N
    68              WRITE (6,103) RR(I),NO(I),FTOT(I)
    69              WRITE (7,103) RR(I),NO(I),FTOT(I)
    70        5     CONTINUE
    71        103   FORMAT (F10.2,I10,F20.5)
    72              STOP
    73              END
END OF FILE
```

A continuous approximation to this N(J) distribution necessitates determining a suitable average value for the interference term in equation 1-10. As the distribution of nearest donors is calculated as a function of log(J) rather than J, we calculated $\log\left(\sum_n^1 \cos(\underline{k}_o^{(n)} \cdot \underline{r})\right)^2$, and obtained the appropriate average value of $\left(\sum_n^1 \cos \underline{k}_o^{(n)} \cdot \underline{r}\right)^2$ to be .4663. Writing J as a continuous function of r, and assuming the nearest donor distribution given by equation , the probability N(J) that a nearest donor pair has exchange energy in the range $J, J + dJ$ is given by:

$$N(J)\, dJ = \frac{4\pi N_d r^2 e^{-\frac{4\pi N_d r^3}{3}}}{(dJ/dr)} \quad dJ \qquad \text{(A-3-6)}$$

Therefore, upon integrating A-3-6 over a certain range of J (the same intervals as in the discrete calculation are used) one should obtain a reasonable approximation to the discrete distribution. This procedure is performed by Program II, where J is denoted by X, and dJ/dr by XP. The resulting probability as calculated from equation A-3-6 is entered into the array PNJ, which the second section of the program integrates over the intervals of J.

PROGRAM II

```
$LIS NOJ2
      1      C       THIS PROG. CALCS.THE FRACT. # OF NRST. DONOR PRS. HAVING
      2      C       EXCHANGE ENERGY "J" FROM A POISSON DIST. OF NRST. DONORS.
      3             READ (5,100) N,AD,CON,RMIN,RMAX
      4      100    FORMAT (I10,F10.2,E10.2,2F10.2)
      5             LOGICAL L1,L2
      6
      7
      8             N=300
      9             DIMENSION ALJ(600),PNJ(600),PJ(600)
     10             DIMENSION RR(600)
     11             REAL LJ(600)
     12             DO 20 I=1,600
     13             PNJ(I)=0.0
     14      20     CONTINUE
     15             AA=2.90E08
     16             BB=2./9.
     17             CC=1./45.
     18             F=.4663
     19             DELR=(RMAX-RMIN)/N
     20             DO 1 I=1,N
     21             R=RMIN+(I-1)*DELR
     22             D=R/AD
     23             FD=AA*BB*(1.+D)*(1.+D+D**2/3.)*EXP(-2.*D)/AD
     24             GD=AA*CC*(25./8.-5.75*D-3.*D**2-D**3/3.+6./D*(1.+D+D**2/3.)*
     25            2(.57722+ALOG(D)))*EXP(-2.*D)/AD
     26             X=F*(FD-GD)
     27             XP=-2*X/AD+F*AA*EXP(-2.*D)/AD**2*(BB*((1+2*D/3)*(1+D)+
     28            2(1+D+D**2/3))-CC*(-5.75-6*D-D**2-6/D**2*(1+D+D**2/3)**2*
     29            3(-.42278+ALOG(D))+12/D*(1+D+D**2/3)*(1+2*D/3)*(.577+ALOG(D))
     30            4)
     31
     32             ALJ(I)=ALOG10(X)
     33             PNJ(I)=-4.*3.1416*CON*R**2*EXP(-4./3.*3.1416*CON*R**3)/XP
     34             WRITE (7,101) R,ALJ(I),PNJ(I)
     35      101    FORMAT (2F20.2,E20.5)
     36      1      CONTINUE
```

```
      PJ(1)=0.
      DO 2 I=1,200
      LJ(I)=(80.-I)/10.
      DO 10 J=1,N
      L1=LJ(I).LE.ALJ(J)
      L2=LJ(I).GE.ALJ(J+1)
      IF (L1.AND.L2) GO TO 11
10    CONTINUE
11     CONTINUE
      IF (ALJ(J).EQ.0.) GO TO 21
      PJ(I)=(LJ(I)-ALJ(J))*(PNJ(J+1)-PNJ(J))/(ALJ(J+1)-ALJ(J)
     2)+PNJ(J)
      GO TO 22
21    CONTINUE
      PJ(I)=0.
22    CONTINUE
      WRITE (6,102) I,LJ(I),PJ(I)
102   FORMAT (I10,F10.3,E20.5)
2     CONTINUE
      STOP
      END
      REAL LJ(600),J(600),NJ(600),JO,LGE,LLJ(200)
      NA=10

      DIMENSION PNJ(200)
      COMMON PNJ,LLJ

      DO 202 I=1,200
      READ (5,200) K,LLJ(I),PNJ(I)
200   FORMAT (I10,F10.3,E20.5)
202   CONTINUE

      N=200
      LGE=ALOG10(2.71828)
      LJ(1)=80.

      J(1)=EXP(LJ(1)/(10.*LGE))
      AREA=0.
      DO 1 I=1,200
      LJ(I+1)=80-I
      J(I+1)=EXP(LJ(I+1)/(10.*LGE))
      CALL SIMP (J(I),J(I+1),NA,NJ(I),CON,JO,ALPHA,M,T)
      AREA=AREA+NJ(I)
      WRITE (6,101) J(I),J(I+1),LJ(I),LJ(I+1),NJ(I)
101   FORMAT (2E10.2,2F10.2,1PE10.2)
1      CONTINUE
      WRITE (6,102) AREA
102   FORMAT (//'AREA UNDER CURVE =',F10.4)
      STOP
      END
END OF FILE
```

APPENDIX D

CALCULATION OF THE THEORETICAL SPECTRUM

This calculation was performed by Program III. The basic operations involved consisted of breaking up the energy into intervals, contained in the array E, calculating the corresponding intervals of exchange energy which were entered into the array J, and subsequently integrating the expression given by equation 2-17 over these intervals of J to obtain the array A. Special attention was given to points for which $E = g\beta H_0$ and $E = g\beta H_0 \pm A/2$ as the exchange energy, written as a function of energy, suffers discontinuities at these points. The elements of the array A were then equated to the areas under the Gaussian shape functions given in equation 2-17, and the height of the hyperfine lines and centre line obtained as their convolution. The value of the ratio of centre to average hyperfine line was then obtained as RATIO. The continuous N(J) courve for a particular concentration and effective Bohr radius as calcualted by Program II was read into Program III as the array LLJ, PNJ.

PROGRAM III

```
$LIS FINAL
      1            LOGICAL L1,L2,L3,LX
      2            DIMENSION E(802),A(802)
      3            REAL J(802),JX(11),        LJ(600),JO,JH(21)
      4            DATA N,NX,NH,B/20,50,50,118./
      5      31    CONTINUE
      6            READ (5,105) CON ,JO,ALPHA,AD,RMAX,T
      7            IF (CON.EQ.0.E0) GO TO 30
      8            DIMENSION PNJ(200)
      9            REAL LLJ(200)
     10            COMMON PNJ,LLJ
     11            DO 202 I=1,200
     12            READ (4,201) K,LLJ(I),PNJ(I)
     13      202   CONTINUE
     14      201   FORMAT (I10,F10.3,E20.5)
     15      105   FORMAT (2E10.2,4F10.4)
     16            DO 1 I=1,802
     17            E(I)=9799.5+FLOAT(I)*.5
     18            IF (E(I).EQ.1.E 04) GO TO 2
     19            J(I)=ABS(B**2/(4.*(E(I)-1. E 04))-E(I)+1.E04)
     20            GO TO 7
     21      2     J(I)=EXP(LLJ(1)/ALOG10(2.71828))
     22      7     CONTINUE
     23            E(I)=E(I)+.25
     24      1     CONTINUE
     25            J(283)=EXP(LLJ(200)/ALOG10(2.71828))
     26            J(519)=J(283)
     27            DO 3 I=1,802
     28            L1=E(I).GE.9941.
     29            L2=E(I).GE.10000.
     30            L3=E(I).GE.10059.
     31            IF (.NOT.L1) M=1
     32            IF (L1.AND..NOT.L2) M=2
     33            IF (L2.AND..NOT.L3) M=3
     34            IF (L3) M=4
     35            LX=(I.EQ.282).OR.(I.EQ.283).OR.(I.EQ.400).OR.(I.EQ.401)
     36           2.OR.(I.EQ.518).OR.(I.EQ.519)
     37            IF (LX) GO TO 5
     38            CALL SIMP (J(I),J(I+1),N,A(I),CON,JO,ALPHA,M,T)
     39            GO TO 3
     40      5     A(I)=0.
     41            JX(1)=AMIN1(J(I),J(I+1))
     42            DO 10 K=1,10
     43            X=ALOG(AMAX1(J(I),J(I+1))/AMIN1(J(I),J(I+1)))*FLOAT(K)/10.
     44            JX(K+1)=AMIN1(J(I),J(I+1))*EXP(X)
     45            CALL SIMP (JX(K),JX(K+1),NX,AX,CON,JO,ALPHA,M,T)
     46            A(I)=A(I)+AX
     47      10    CONTINUE
     48      3     CONTINUE
     49            HYP=0.
     50            JH(1)=J(283)
```

```
      DO 11 K=1,20
      X=ALOG(J(401)/J(283))*FLOAT(K)/20.
       JH(K+1)=J(283)*EXP(X)
      CALL SIMP (JH(K),JH(K+1),NH,AH,CON,JO,ALPHA,5,T)
      HYP=HYP+AH
11    CONTINUE
      HHBL=0.
      DO 12 I=263,303
      HHBL=HHBL+A(I)/(SQRT(2.*3.1416)*8.)*EXP(-.5*((E(283) -E(I))/8.)**2
     2)
12    CONTINUE
      HCL=0.
       DO 13 I=381,421
      HCL=HCL  +A(I)/(SQRT(2.*3.1416)*8.)*EXP(-.5*((E(401) -E(I))/8.)**2
     2)
13    CONTINUE
      HHBR=0.
      DO 14 I=499,539
      HHBR=HHBR+A(I)/(SQRT(2.*3.1416)*8.)*EXP(-.5*((E(519) -E(I))/8.)**2
     2)
14    CONTINUE
      HHL=HYP/(SQRT(2.*3.1416)*8.)
      RATIO=2.*HCL/(2.*HHL+HHBL+HHBR)*100.
      HL=HHL+HHBL
      HR=HHL+HHBR
      WRITE (6,100) AD,JO,ALPHA,CON,T,RMAX
      WRITE (6,102) N,NX,NH,HL ,HCL,HR
      WRITE (6,103) RATIO
      GO TO 31
30    CONTINUE
      STOP
100   FORMAT (///55X,'AD=',F5.1,///1X,'JO=',E10.2,9X,'ALPHA=',
     2F10.3,7X,'CON=',E10.2,9X,'TEMP=',F10.2,8X,'RMAX=',F10.1/)
102   FORMAT (/50X,'CHECKING PARAMETERS',//1X,'N=',I8,38X,'NH=',
     2I8,38X,'NH=',I8,//2X,'HEIGHT OF LEFT HYPERFINE LINE =',1PE10.2,
     3/2X,'HEIGHT OF CENTRE LINE =',8X,E10.2,/2X,
     4'HEIGHT OF RIGHT HYPERFINE LINE =',E10.2/)
103   FORMAT (//2X,'RATIO OF CENTRE LINE TO HYP LINES (BY PERCENT)
     2 ) =',F10.2,///)
      END
      SUBROUTINE SIMP (A,B,N,AREA,CON,JO,ALPHA,M,T)
      REAL JO
      REAL LLJ(200)
      DIMENSION PNJ(200)
      COMMON PNJ,LLJ
      AN = N
      H=(B-A)/AN
      SUM1=0.0
      SUM2=0.0
      CALL AUX (A,Y,CON,JO,ALPHA,M,T)
      YA=Y
      CALL AUX (B,Y,CON,JO,ALPHA,M,T)
      YB=Y
      X = A-H
      NN=N/2
      DO 30 I = 1,NN
      X = X+2.0*H
      CALL AUX (X,Y,CON,JO,ALPHA,M,T)
30    SUM1=SUM1+Y
      X=A
```

```
111             DO 40 I = 2,NN
112             X = X+2.0*H
113             CALL AUX (X,Y,CON,JO,ALPHA,M,T)
114      40     SUM2=SUM2+Y
115             AREA = H/3.0*(YA+4.0*SUM1+2.0*SUM2+YB)
116             AREA=ABS(AREA)
117             RETURN
118             END
119             SUBROUTINE AUX (X,Y,CON,JO,ALPHA,M,T)
120             REAL JO ,MINUS
121             DATA BOL,AH/2.08E4,118./
122
123             REAL LLJ(200)
124             DIMENSION PNJ(200)
125             COMMON PNJ,LLJ
126             ALX=ALOG10(X)
127             IF (ALX.LT.0.) GO TO 300
128             N=80-INT(10.*ALX)
129             IF (N.LE.1) GO TO 302
130             GO TO 301
131      300    CONTINUE
132             N=81-INT(10.*ALX)
133             IF (N.GT.200) GO TO 302
134             GO TO 301
135      302    CONTINUE
136             PJ=0.0
137             GO TO 303
138      301    CONTINUE
139             PJ=-10.*(ALX-LLJ(N-1))*(PNJ(N)-PNJ(N-1))+PNJ(N-1)
140      303    CONTINUE
150             RT=SQRT(X**2+AH**2)
151             PLUS=.5*(1.+X/RT)
152             MINUS=.5*(1.-X/RT)
153             IF (M.GE.2) GO TO 2
154             Y=MINUS*PJ*ABS(1.-EXP((2.E4-X-RT)/(2.*BOL*T)))
155             GO TO 1
156      2      CONTINUE
157             IF (M.GE.3) GO TO 3
158             Y=PLUS*PJ*EXP(-(X+RT)/(2.*BOL*T))*(1.-EXP(-1.E4/(BOL*T)))
159             GO TO 1
160      3      CONTINUE
161             IF (M.GE.4) GO TO 4
162             Y=PLUS*PJ*EXP(-(X+RT)/(2.*BOL*T))*(EXP(1.E4/(BOL*T))-1.)
163             GO TO 1
164      4      CONTINUE
165             IF (M.EQ.5) GO TO 5
166             Y=MINUS*PJ*(1.-EXP(-(2.E4+X+RT)/(2.*BOL*T)))
167             GO TO 1
168      5      CONTINUE
169             Y=.5*PJ*EXP(-(X+RT)/(2.*BOL*T))
170            2*(EXP(1.E4/(BOL*T))-EXP(-1.E4/(BOL*T)))
171      1      CONTINUE
172             RETURN
173             END
END OF FILE
```